VRIJE
UNIVERSITEIT
BRUSSEL

Comparative study on the effects of alkylsilyl and alkylthio side chains on the performance of fullerene and non-fullerene polymer solar cells

Genene, Zewdneh; Negash, Asfaw; Abdulahi, Birhan A.; Eachambadi, Raghavendran Thiruvallur; Liu, Zhen; Van den Brande, Niko; D'Haen, Jan; Wang, Ergang; Vandewal, Koen; Manca, Jean; Mammo, Wendimagegn; Admassie, Shimelis

Comparative study on the effects of alkylsilyl and alkylthio side chains on the performance of fullerene and non-fullerene polymer solar cells

Zewdneh Genene[ab†], Asfaw Negash[ac†*], Birhan A. Abdulahi[ad], Raghavendran Thiruvallur Eachambadi[e], Zhen Liu[f], Niko Van den Brande[f], Jan D'Haen[c], Ergang Wang[d], Koen Vandewal[c], Wouter Maes[c*], Jean Manca[e], Wendimagegn Mammo[a], Shimelis Admassie[ag]

[a] Department of Chemistry, Addis Ababa University, P.O. Box 33658, Addis Ababa, Ethiopia

[b] Department of Chemistry, Ambo University, P.O. Box 19, Ambo, Ethiopia

[c] Institute for Materials Research (IMO-IMOMEC), Hasselt University, Agoralaan 1 – Building D, 3590 Diepenbeek, Belgium

[d] Department of Chemistry and Chemical Engineering, Chalmers University of Technology, SE-412 96 Göteborg, Sweden

[e] X-LAB, Hasselt University, Universitaire Campus, Agoralaan 1, 3590 Diepenbeek, Belgium

[f] Physical Chemistry and Polymer Science (FYSC), Vrije Universiteit Brussel (VUB), Pleinlaan 2, 1050 Brussels, Belgium

[g] State Key Laboratory of Luminescent Materials and Devices, Institute of Polymer Optoelectronic Materials and Devices, School of Materials Science and Engineering, South China University of Technology, 381 Wushan Road, Guangzhou 510640, P.R. China

[†] These authors contributed equally to this work.

[*] asfaw.negashassegde@uhasselt.be; wouter.maes@uhasselt.be

Abstract

Two novel high gap donor polymers – **PBDTTSi-TzBI** and **PBDTTS-TzBI**, based on imide fused benzotriazole (TzBI) with asymmetric side chains and alkylsilyl (Si) or alkylthio (S) substituted 4,8-di(thien-2-yl)benzo[1,2-*b*:4,5-*b'*]dithiophene (BDTT) – are successfully synthesized. The effect of the side chain variation on the photophysical, morphological and photovoltaic properties of blends of these polymers with fullerene and non-fullerene acceptors is investigated. The **PBDTTSi-TzBI** polymer shows a deeper highest occupied molecular orbital energy level, which results in higher open-circuit voltages. Nevertheless, the polymer solar cells fabricated using **PBDTTS-TzBI** in combination with $PC_{71}BM$ afford a higher power conversion efficiency of 7.3% (vs 4.0% for **PBDTTSi-TzBI**:$PC_{71}BM$). By using the non-fullerene acceptor ITIC, the absorption of the blends extends to 850 nm and better device efficiencies are achieved, 6.9% and 9.6% for **PBDTTSi-TzBI**:ITIC and **BDTTS-TzBI**:ITIC, respectively. The better performance for **PBDTTS-TzBI**:ITIC is attributed to the strong and broad absorption and balanced charge transport, and is among the best so far for non-fullerene solar cells based on TzBI-containing polymer donors.

Introduction

Polymer solar cells offer specific advantages, such as low weight, attractive colors, semitransparency, solution processability and good compatibility with flexible substrates.[1-5] They generally contain bulk heterojunction (BHJ) photoactive layers composed of intermixed electron donor and acceptor materials. Historically, fullerenes have been widely used as acceptors and power conversion efficiencies (PCEs) up to 11.7% have been realized for single junction polymer:fullerene solar cells (12.1% for ternary devices) through optimal material design, blend morphology control and device engineering.[6, 7] However, further improvement of the performance of fullerene-based polymer solar cells and their practical applications are hampered by their limited molecular absorption and energy level variability, and the high production and purification costs of fullerene derivatives. Moreover, the resulting devices often show high energy losses and morphological instability.[8, 9] To address these issues, non-fullerene acceptors (NFAs) have recently appeared as more promising alternatives. Unlike fullerenes, these acceptors show strong absorption in the visible up to the near-infrared (NIR) region, adjustable energy levels and enhanced morphological stability and lower energy losses when combined in BHJ blends.[10-12] In the last few years, several NFAs have been developed that rival and even outperform fullerene-based acceptors when combined with certain donor materials.[13-18] The majority of NFAs are low gap small molecules with a 'pull-push-pull' (or acceptor-donor-acceptor) structure, such as ITIC and its derivatives.[17, 19, 20] At present, non-fullerene polymer solar cells have reached impressive PCEs of around 16% for single junction[21, 22] and even over 17% for tandem devices.[23]

Alongside the rapid development of NFAs, suitable donor polymers with complementary absorption and properly aligned energy levels are required to achieve high performance. High gap polymers (i.e. optical gap above 1.8 eV) are typically used to complement NFAs, which show strong absorption in the lower energy region. These donor polymers are developed based on the well-known push-pull approach, which combines moderately electron-rich and electron-deficient building blocks in an alternating fashion. This strategy is used to easily tune the absorption and energy levels through intramolecular charge transfer from the push to the pull units.[24, 25]

Benzotriazole is one of the widely used electron-pulling building blocks for the synthesis of both high gap polymers and NFAs.[26-34] Imide-fused benzotriazoles, in particular pyrrolo[3,4-

3

f]benzotriazole-5,7(6*H*)-dione (TzBI), have recently been employed as moderately electron-deficient pull units for the construction of high gap polymers. The cyclic imide moiety concurrently lowers both the highest occupied molecular orbital (HOMO) and the lowest unoccupied molecular orbital (LUMO) energy levels of the resulting polymers, which is beneficial for the open-circuit voltage (V_{oc}) and the efficiency of polymer solar cells.[35, 36] In addition, the nitrogen atom of the imide also provides a facile pathway for alkylation to optimize the polymer solubility and aggregation tendency. Most of the TzBI-containing high gap polymers reported so far have linear octyl side chains attached on both the imide and the benzotriazole.[37, 38] Little attention has been devoted to TzBI units with asymmetric side chains. Recently, Cao *et al*. reported a high gap polymer based on TzBI bearing a linear octyl side chain on the imide and a branched alkyl side chain on the benzotriazole unit.[39] This polymer showed a PCE of 6.1% when blended with ITIC and an excellent efficiency above 12% with IT-2F as the acceptor.

Besides the electron-deficient units, the electron-rich building blocks and the side chains also play a critical role in modulating the optical absorption, energy levels, charge transport properties and BHJ blend morphology.[40-42] Thus far, the 4,8-di(thien-2-yl)benzo[1,2-*b*:4,5-*b′*]dithiophene (BDTT) unit has been most commonly used as the electron-rich building block to construct high performance push-pull copolymers.[43-45] In fact, most of the high-efficiency non-fullerene polymer solar cells are constructed using donor polymers derived from BDTT units.[21, 46] It has been shown that the introduction of alkylthio side chains on the BDTT unit is an effective strategy to down-shift the HOMO energy levels and thereby enhance the V_{oc} in polymer solar cells, which is attributed to the π-electron withdrawing ability of divalent sulfur from the p-orbital of the carbon-carbon double bond into its empty 3d-orbitals.[47-50] The alkylthio side chains also enhance the polymer crystallinity and mobility and thereby lead to high performances.[51] Recently, Peng *et al*.[52] reported non-fullerene solar cells based on an alkylthio-functionalized BDTT-based polymer and ITIC (E_g~1.59 eV), which showed a notable V_{oc} of 1.1 V, a large short-circuit current density (J_{sc}) of 17.78 mA cm^{-2} and a high PCE of 12.8%. On the other hand, the HOMO energy levels have also been lowered by introducing alkylsilyl side chains on the BDTT unit, due to the interaction of the σ* orbitals of the Si atoms with the π* orbitals of the aromatic units.[53-55] The alkylsilyl side chains seem to facilitate a planar geometry of the polymer backbone to enhance crystallinity.[56, 57] The first trialkylsilyl-substituted 2D-conjugated polymer

(J71) was reported by Li *et al.* in 2016 and afforded a PCE of 11.4% when blended with ITIC and applied in BHJ organic solar cells, with a high V_{oc} of 0.94V.[32] However, an inclusive comparison of high gap polymers with alkylthio and alkylsilyl side chains and their effect on blend morphology and photovoltaic performance of fullerene and non-fullerene polymer solar cells has not been reported hitherto.

Herein, we present the design and synthesis of two new high gap polymers, **PBDTTSi-TzBI** and **PBDTTS-TzBI** (Scheme 1), based on a BDTT monomer containing alkylsilyl or alkylthio side chains, respectively. The impact of the side chains on the BHJ film morphology and photovoltaic performance is analyzed. **PBDTTSi-TzBI** exhibits a lower HOMO level and a higher V_{oc} in polymer solar cells. However, **PBDTTS-TzBI** shows a broader and stronger absorption. When $PC_{71}BM$ is used as the electron acceptor, a PCE of 7.3% is achieved for **PBDTTS-TzBI**, while significantly less efficient devices (4.0%) are obtained for **PBDTTSi-TzBI**. Non-fullerene solar cells based on both polymers give higher performances. The results obtained from both inverted and conventional devices confirm that the solar cells based on **PBDTTS-TzBI** afford a higher external quantum efficiency (EQE, up to 79%) and higher PCEs. The **PBDTTS-TzBI**:ITIC devices fabricated from chlorobenzene solution with 0.2% diphenyl ether (DPE) as a processing additive and thermal annealing at 130 °C show a PCE of 9.6% as a result of strong and broad absorption and balanced charge transport.

Results and discussion

The Stille cross-coupling polymerization reactions affording **PBDTTSi-TzBI** and **PBDTTS-TzBI** are depicted in Scheme 1. The experimental details can be found in the Supplementary data file. The pull monomer TzBI was synthesized by a reported procedure.[35] The 2-ethylhexyl and octyl side chains were selected to ensure good solubility and to achieve a reasonably high molar mass. The push monomer BDTTSi was also synthesized following a reported method.[58] The polymers were purified by successive Soxhlet extractions with acetone, diethyl ether and chloroform. For **PBDTTS-TzBI**, only a limited amount of polymer could be extracted with chloroform and further treatment with *ortho*-dichlorobenzene was required to recover most of the polymer material. **PBDTTSi-TzBI** appeared to be more soluble, as observed before for polymers with alkylsilyl side chains.[58] The number-average molar masses (M_n) of **PBDTTS-TzBI** and **PBDTTSi-TzBI** were determined to be 28.1 and 59.7 kDa, respectively, by high-temperature gel

permeation chromatography (Table 1). For the alkylthio polymer, a batch with lower M_n (14.7 kDa) was recovered as well (from the chloroform extract). All further analysis was conducted on the high molar mass batch of **PBDTTS-TzBI**.
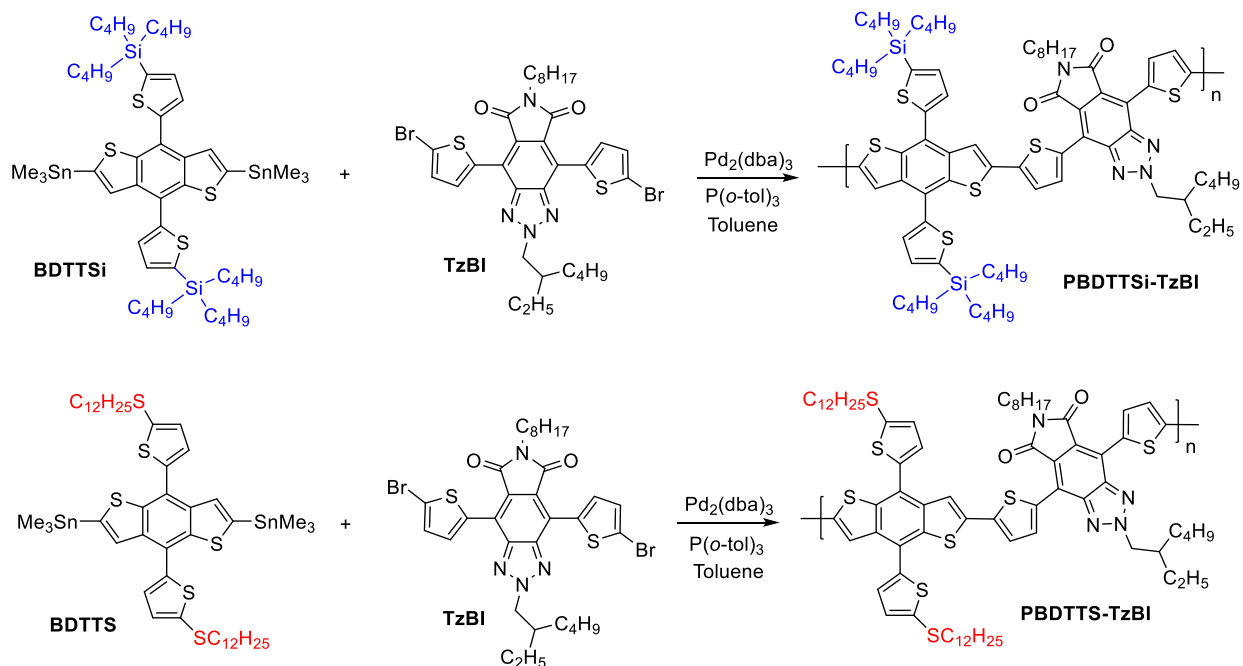

Scheme 1. Polymerization reactions toward **PBDTTSi-TzBI** and **PBDTTS-TzBI**.

The thermal stabilities of the polymers were investigated by thermogravimetric analysis (TGA). The decomposition temperatures (associated with the onset of mass loss) of **PBDTTSi-TzBI** and **PBDTTS-TzBI** were determined to be ~410 and 315 °C, respectively (Figure S1). The enhanced thermal stability of **PBDTTSi-TzBI** is one of the merits of alkylsilyl side chains.[58]

To study the effects of the side chains on the optical properties, UV-Vis-NIR absorption spectra were recorded both in chloroform solution and in the solid state (Figure 1, Table 1). Going from solution to film, the absorption maxima red-shift by 42 nm for **PBDTTSi-TzBI** and 15 nm for **PBDTTS-TzBI**, respectively, which can be ascribed to (π-π) intermolecular interactions in the solid state.[42] Relatively weak shoulders can be observed for both polymers at the low energy side. The long wavelength absorption maximum of **PBDTTS-TzBI** is red-shifted by 16 nm compared to that of **PBDTTSi-TzBI**. The absorption coefficient of **PBDTTS-TzBI** in solution is also somewhat higher (Table 1, Figure 1), which can be related to the auxochromic effect of the alkylthiol side chains, for which the lone pairs of electrons on the sulfur atoms can extend the

conjugated system.[59] Thus, photoactive layers based on **PBDTTS-TzBI** can absorb more solar photons, which is potentially beneficial for the J_{sc} of polymer solar cells. The absorption onsets of the polymer films are 693 and 660 nm, corresponding to optical gaps (E_g^{op}) of 1.79 and 1.88 eV for **PBDTTS-TzBI** and **PBDTTSi-TzBI**, respectively. This clearly illustrates that replacing the alkylthiol with alkylsilyl side chains increases the optical gap of the polymer. Moreover, the absorption of both donor polymers nicely complements that of the ITIC acceptor (Figure 1), which is valuable to broaden the absorption and harvest more photons in the projected solar cell devices. The absorption spectra of the donor: acceptor blends are depicted in Figure S2.
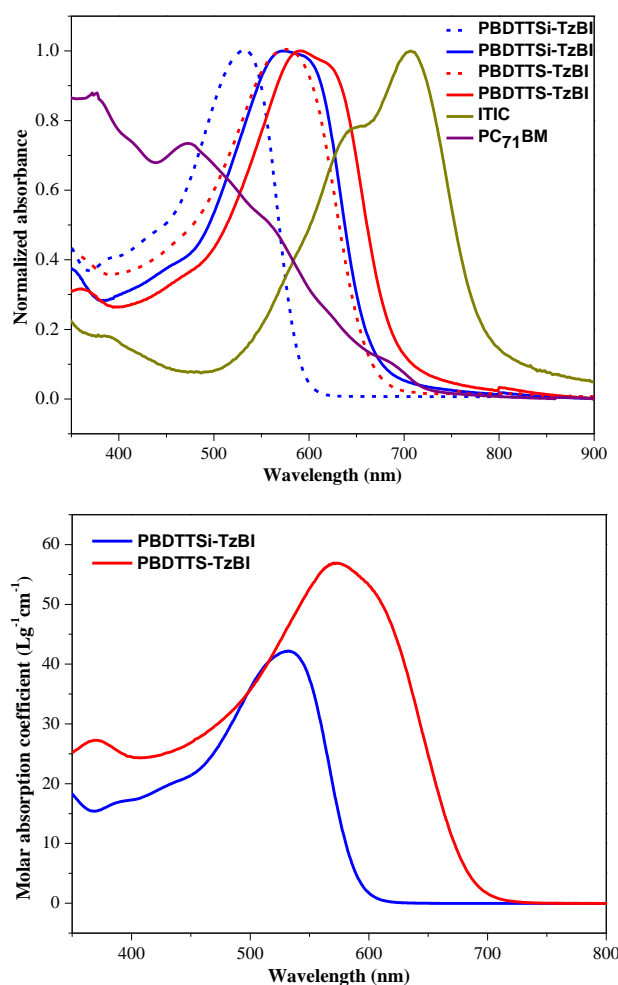

Figure 1. (top) UV-Vis-NIR absorption spectra of **PBDTTSi-TzBI** and **PBDTTS-TzBI** in chloroform solution (dashed lines) and thin film (solid lines), together with the spectra of ITIC and PC$_{71}$BM in film. (bottom) Molar absorption coefficients for **PBDTTSi-TzBI** and **PBDTTS-TzBI** in chloroform solution.

Table 1. Molar mass (distribution), optical and electrochemical properties of the polymers.

Polymer	M_n [kDa]	$Đ$	λ_{max} [nm] Solution	film	ε (Lg^{-1}cm^{-1})	E_g^{op} [eV]	HOMO [eV]	LUMO [eV]	E_g^{CV} [eV]
PBDTTSi-TzBI	59.7	2.6	532	574	43	1.88	−5.46	−3.33	2.13
PBDTTS-TzBI	28.1	2.8	575	590	57	1.79	−5.38	−3.32	2.06

The energy levels of the two polymers (Figure 2, Table 1) were estimated by cyclic voltammetry (CV) experiments on films of the two materials (Figure S3). The HOMO/LUMO energy levels were determined from the onset potentials of oxidation and reduction to be −5.46/−3.33 eV for **PBDTTSi-TzBI** and −5.38/−3.32 eV for **PBDTTS-TzBI**, resulting in electrochemical gaps (E_g^{CV}) of 2.13 and 2.06 eV, respectively. This indicates that the tri-*n*-butylsilyl side chains effectively lower the HOMO level, which is expected to result in an improved V_{oc} in solar cells.
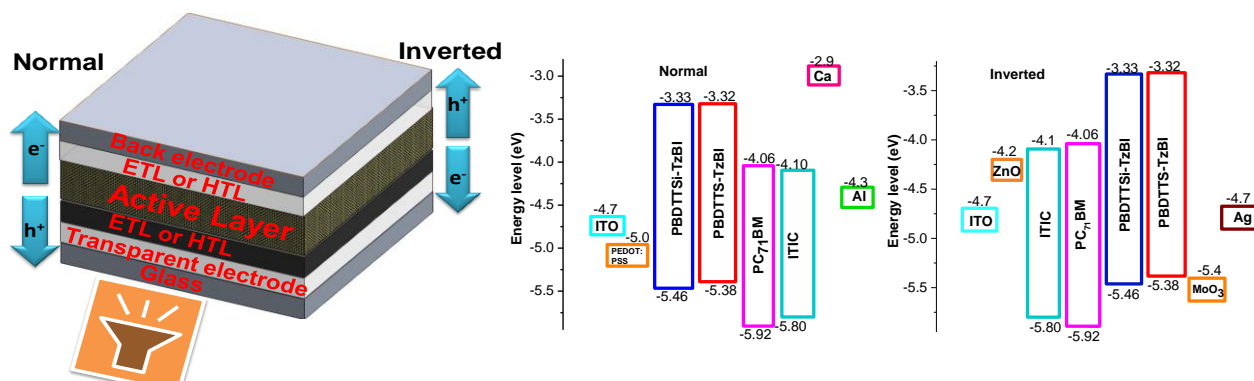
Figure 2. Solar cell device architectures and energy level diagrams for the donor polymers, acceptor materials and interlayers used in the device stacks.[60-62]

To study the effect of the donor polymer side chains on the photovoltaic performance, both fullerene-based and non-fullerene polymer solar cells were fabricated using the inverted device architecture ITO/ZnO/photoactive layer/MoO$_3$/Ag, wherein the photoactive layer consisted of **PBDTTSi-TzBI** or **PBDTTS-TzBI** as the donor and PC$_{71}$BM or ITIC as the acceptor. The device performances were optimized by varying the donor to acceptor weight ratio, processing solvent and additive, thermal annealing temperature and thickness of the active layer. Details of the performance optimization are provided in Tables S1−S3. The current density-voltage (*J-V*)

and EQE curves for the best devices are depicted in Figure 3 and their photovoltaic data are summarized in Table 2.
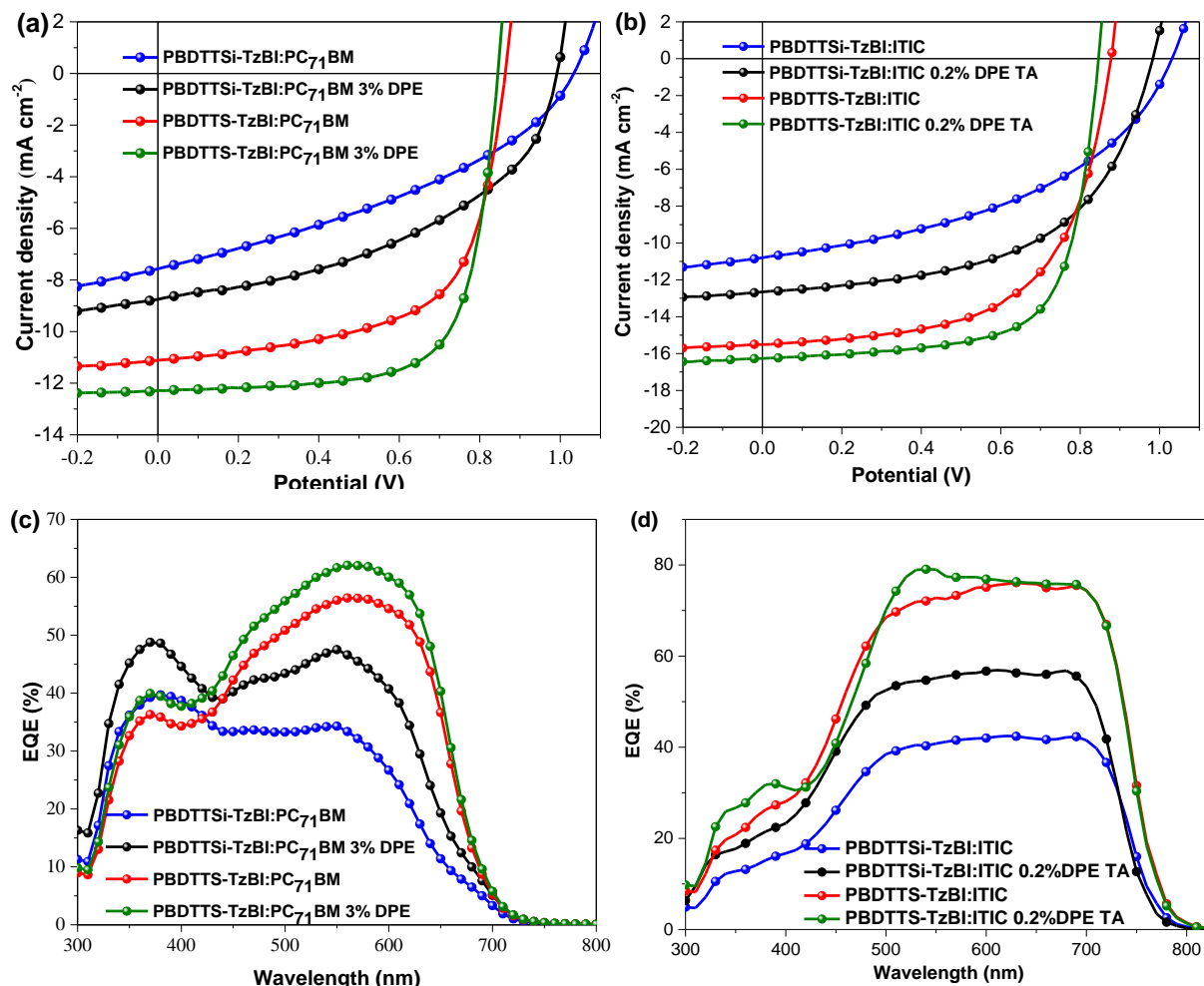
Figure 3. (a,b) *J-V* characteristics and (c,d) EQE spectra for the (inverted) polymer solar cells based on polymer:$PC_{71}BM$ and polymer:ITIC blends.

The polymer solar cells based on **PBDTTS-TzBI**:$PC_{71}BM$ fabricated without processing additive showed a PCE of 6.02%, which is higher than the PCE obtained from **PBDTTSi-TzBI**:$PC_{71}BM$ (2.93%). These PCEs increase when 3% of DPE is used as a processing additive. The **PBDTTS-TzBI**:$PC_{71}BM$ devices exhibit an increased FF of 0.71, resulting in a higher PCE of 7.32%. Although the **PBDTTSi-TzBI**:$PC_{71}BM$ solar cells gave a higher V_{oc} of 0.99 V, the lower J_{sc} and FF lead to a significantly lower final efficiency (3.98%). As anticipated, a higher V_{oc} was obtained for the **PBDTTSi-TzBI**-based devices.

9

Table 2. Photovoltaic parameters for the optimized polymer solar cells.

| Active layer	Additive (DPE)[a]	Thickness [nm]	V_{oc} [V]	J_{sc} [mA cm^{-2}]	FF	PCE [%][c]	E_{loss} [eV]
PBDTTSi-TzBI:PC$_{71}$BM	-	130±3	1.02	7.57	0.38	2.93 (2.68±0.17)	1.13
	3%	128±2	0.99	8.75	0.46	3.98 (3.85±0.15)	1.09
PBDTTS-TzBI:PC$_{71}$BM	-	145±2	0.86	11.11	0.63	6.02 (5.88±0.11)	1.11
	3%	142±3	0.84	12.28	0.71	7.32 (7.26±0.12)	1.15
PBDTTSi-TzBI:ITIC	-	116±2	1.03	10.80	0.44	4.90 (4.74±0.16)	0.69
	0.2%	112±3	1.00	12.66	0.50	6.33 (6.05±0.16)	0.73
	0.2% + TA	112±4	0.98	12.70	0.55	6.85 (6.63±0.20)	0.79
	0.2% + TA[b]	105±2	1.00	12.05	0.50	6.03 (5.92±0.09)	0.74
PBDTTS-TzBI:ITIC	-	115±2	0.86	15.51	0.61	8.14 (8.03±0.10)	0.87
	0.2%	114±3	0.86	16.22	0.65	9.07 (8.91±0.15)	0.87
	0.2% + TA	112±2	0.85	16.36	0.69	9.60 (9.30±0.14)	0.89
	0.2% +TA[b]	107±3	0.86	15.81	0.65	8.84 (8.76±0.11)	0.87

[a] DPE = diphenyl ether, TA = thermal annealing (at 130 °C). [b] Conventional device architecture. [c] Best efficiencies. The average PCE and standard deviation values (in brackets) were calculated from 8−16 devices.

Although PCEs over 7% were achieved, the rather narrow absorption of the polymer:PC$_{71}$BM blends (Figure S2) presents a limitation to the J_{sc} and efficiency of these devices. The absorption features look more promising for the polymer:ITIC films, which demonstrate complementary absorption extended into the NIR, promoting photon harvesting. It was found that the non-fullerene solar cells demonstrate similar trends as the fullerene-based devices. Without processing additive and post-treatment, the **PBDTTS-TzBI**:ITIC device gave a PCE of 8.14%, with a V_{oc} of 0.86 V, a J_{sc} of 15.51 mA cm^{-2} and a FF of 0.61. When using 0.2% DPE as a

processing additive, the J_{sc} and FF enhanced to 16.22 mA cm^{-2} and 0.65, respectively, while the V_{oc} remained unchanged (Figure S4). Thus, the PCE increased to 9.07%. After thermal annealing (TA) at 130 °C, the **PBDTTS-TzBI**-based devices yielded the best photovoltaic performance, with a notable PCE of 9.6%, among the highest efficiencies achieved with TzBI-based donor polymers.[38, 39, 63, 64] The high performance of **PBDTTS-TzBI** in non-fullerene solar cells can be attributed to its high molar absorption coefficient (see Figure 1), broad blend absorption, reasonably high and balanced charge carrier mobilities as well as increased charge dissociation and transport (as discussed below). On the other hand, the **PBDTTSi-TzBI**:ITIC devices showed a lower maximum efficiency of 6.85% after addition of 0.2% DPE and thermal annealing at 130 °C (Figure 3, S4). The lower performance can be attributed to the lower J_{sc} and FF, despite the higher V_{oc}. For the **PBDTTS-TzBI** polymer, non-fullerene solar cells were also prepared from the lower molar mass batch, affording (slightly) lower device efficiencies (Table S5, Figure S6). EQE spectra (Figure 3c, d) confirm that the ITIC-based solar cells exhibit a broader response up to 800 nm and a particularly strong response from 450 up to 750 nm (see direct comparison in Figure S7). The EQE spectra clearly show that both the donor polymers and the acceptors contribute to photon harvesting, with ITIC contributing more than PC$_{71}$BM, which leads to higher J_{sc} values for the non-fullerene devices. More specifically, the **PBDTTS-TzBI**:ITIC solar cells showed an EQE up to 79% at 540 nm. The higher EQE responses of the **PBDTTS-TzBI**-based devices are consistent with the J_{sc} values as obtained from *J-V* measurements.

Finally, non-fullerene polymer solar cells with a conventional device structure glass/ITO/PEDOT:PSS/polymer:acceptor/Ca/Al were also fabricated (Table 2, Table S4, Figure S5). Similar to the inverted devices, also here the **PBDTTS-TzBI**:ITIC devices showed the highest PCE, 8.84%, under optimized conditions, whereas the **PBDTTSi-TzBI**:ITIC solar cells showed a somewhat lower maximum efficiency of 6.03%. Also here, a higher V_{oc} was recorded for the devices made from **PBDTTSi-TzBI**.

Atomic force microscopy (AFM) and transmission electron microscopy (TEM) experiments were then carried out to investigate the effects of the alkylthio and alkylsilyl side chains on the morphologies of the photoactive layers (Figure 4). The root-mean-square (RMS) roughness values of the **PBDTTSi-TzBI**:ITIC and **PBDTTS-TzBI**:ITIC blend films processed without additive are 0.91 and 1.04 nm, respectively. Upon addition of 0.2% DPE and thermal annealing at 130 °C, the RMS values reduced to 0.66 and 0.69 nm, respectively. No particular features

were observed in either the AFM or TEM images (for which a lack of contrast between the two materials can be expected).
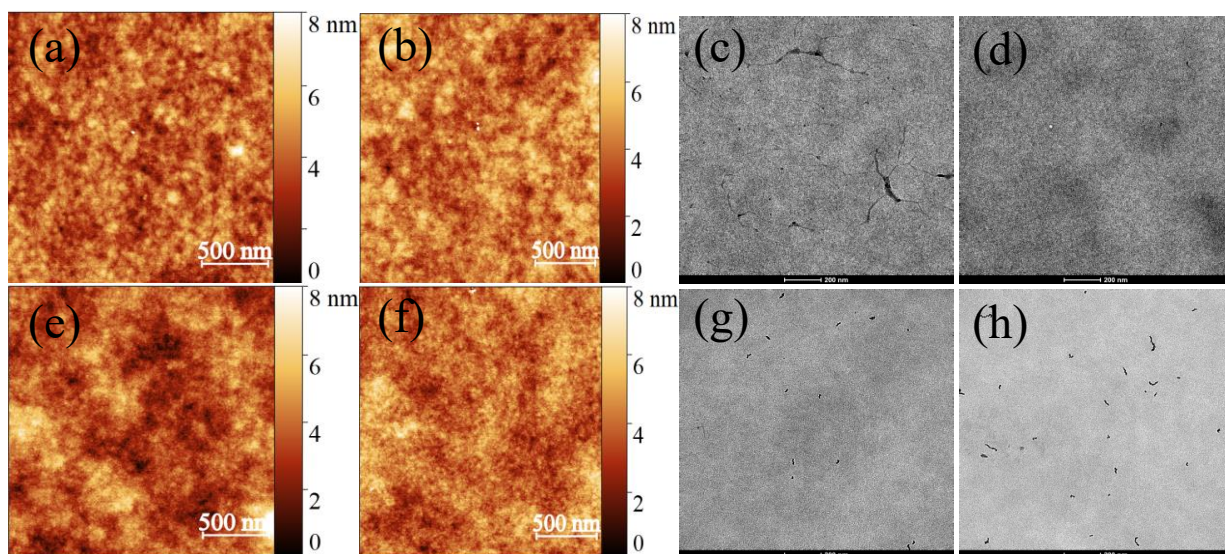

Figure 4. AFM (2×2 μm^2) and TEM (1.5×1.5 μm^2) images of the highest efficiency polymer solar cells based on (a-c) **PBDTTSi-TzBI**:ITIC processed without DPE, (b-d) **PBDTTSi-TzBI**:ITIC processed with 0.2% DPE and thermal annealing at 130 °C, (e-g) **PBDTTS-TzBI**:ITIC processed without DPE, and (f-h) **PBDTTS-TzBI**:ITIC processed with 0.2% DPE and thermal annealing at 130 °C.

The charge carrier mobilities of devices containing **PBDTTS-TzBI** and **PBDTTSi-TzBI** based blends were then measured by the space charge limited current (SCLC) method.[50, 65] Hole-only devices with a configuration ITO/PEDOT:PSS/polymer:ITIC/Au and electron-only devices with a structure ITO/ZnO/polymer:ITIC/Ca/Al were fabricated. The hole/electron mobilities for **PBDTTSi-TzBI**:ITIC and **PBDTTS-TzBI**:ITIC were determined to be $2.15\times10^{-4}/6.12\times10^{-5}$ cm^2 V^{-1} s^{-1} and $6.17\times10^{-4}/4.25\times10^{-4}$ cm^2 V^{-1} s^{-1}, respectively (Figure S8). Under optimized processing conditions, the hole/electron mobilities for **PBDTTSi-TzBI**:ITIC and **PBDTTS-TzBI**:ITIC increased to $5.24\times10^{-4}/1.98\times10^{-4}$ cm^2 V^{-1} s^{-1} and $9.27\times10^{-4}/7.32\times10^{-4}$ cm^2 V^{-1} s^{-1}, respectively. Compared with **PBDTTSi-TzBI**:ITIC, the **PBDTTS-TzBI**:ITIC devices showed slightly higher and more balanced (μ_h/μ_e) charge carrier mobilities, which is in line with the higher J_{sc} and FF values obtained for the solar cells.

The exciton dissociation and charge extraction of the best polymer solar cells were then investigated by measuring the photocurrent density (J_{ph}) *versus* the effective potential (V_{eff}) and the charge collection probability (P_c) (Figure 5). J_{ph} is defined as $J_{ph} = J_L - J_D$, where J_L and J_D are the light and dark current densities, respectively, whereas V_{eff} is defined as $V_{eff} = V_0 - V_a$, with V_0 the potential at $J_{ph} = 0$ and V_a the applied potential.[66] As shown in Figure 5a, the J_{ph} of the polymer solar cells derived from **PBDTTSi-TzBI** and **PBDTTS-TzBI** reached the saturation current density (J_{sat}) in the high-potential region (≥ 2 V). The P_C of the **PBDTTSi-TzBI**:ITIC and **PBDTTS-TzBI**:ITIC devices was evaluated using the formula $P_C = J_{ph}/J_{sat}$, from which the P_C values under short-circuit conditions were calculated to be 88 and 97%, respectively. This indicates that the exciton dissociation, charge extraction and charge collection of the **PBDTTS-TzBI**:ITIC devices are more efficient, which is consistent with the higher EQE, J_{sc} and FF.[66, 67] The results show that the incorporation of alkylthio side chains facilitates charge dissociation in the blends.

Furthermore, photoluminescence (PL) quenching experiments were conducted to further elucidate the exciton dissociation and charge-transfer behavior in the non-fullerene blends (Figure 6). The excitation wavelengths for the pristine donor polymers **PBDTTSi-TzBI** and **PBDTTS-TzBI** were 580 and 600 nm, respectively, while that for ITIC was 700 nm. The pure donor polymers exhibited strong PL. For the **PBDTTSi-TzBI**:ITIC and **PBDTTS-TzBI**:ITIC blend films, the emissions were quenched by 85 and 92%, respectively. Upon addition of 0.2% DPE during blend deposition and thermal annealing of the films at 130 °C, the emission of the blend films was even more efficiently quenched, by 91 and 96%, respectively, suggesting effective electron transfer from the polymers to ITIC for the excitons generated in the donor phase.
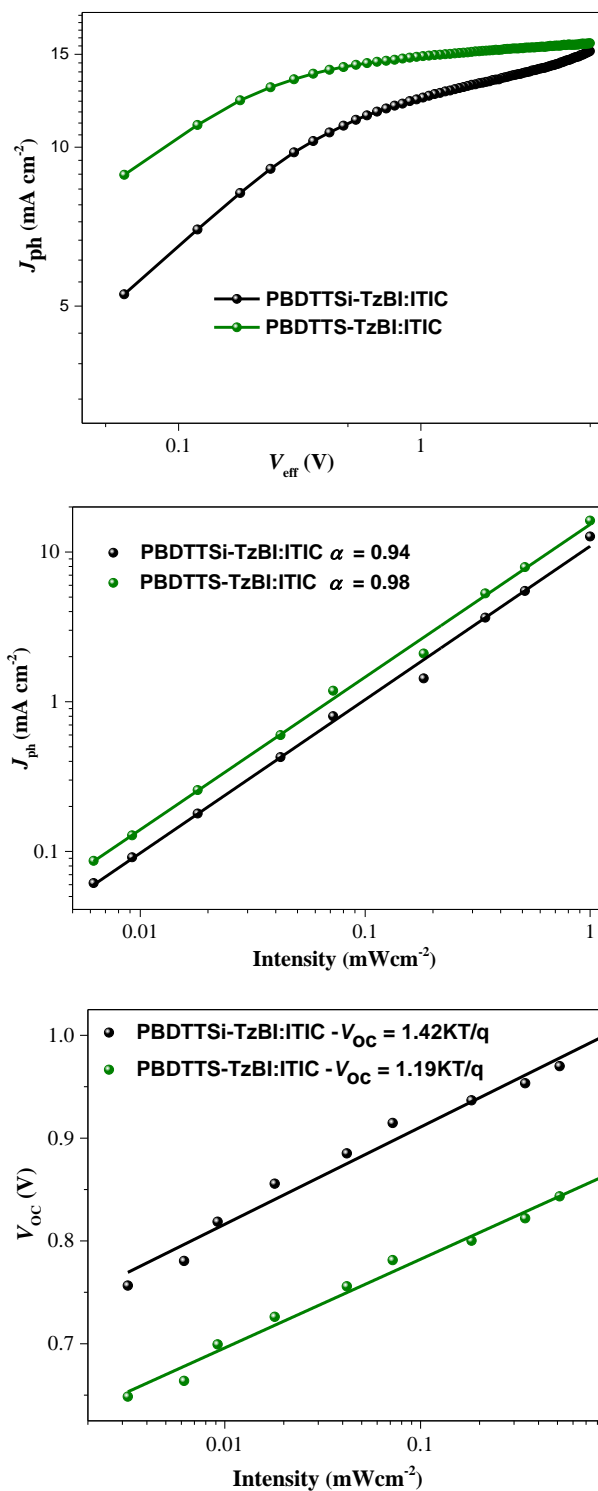
Figure 5. (top) Plot of the photocurrent density (J_{ph}) *versus* the effective potential (V_{eff}). (middle) Dependence of J_{sc} on light intensity. (bottom) Dependence of V_{oc} on light intensity for the best-performing solar cell devices.
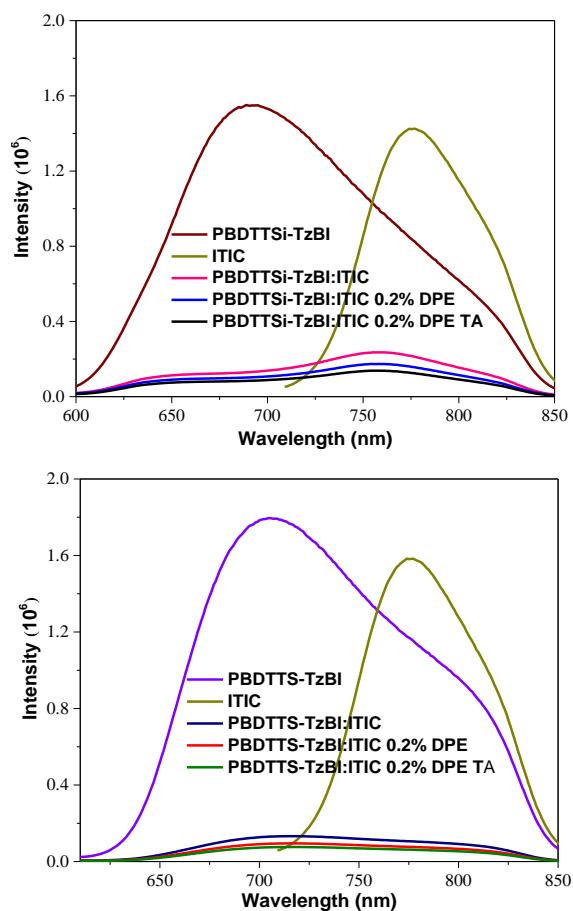
Figure 6. Photoluminescence spectra of the two pristine polymers, ITIC and the corresponding blend films: (top) **PBDTTSi-TzBI** and **PBDTTSi-TzBI**:ITIC films excited at 580 nm and a pure ITIC film excited at 700 nm. (bottom) **PBDTTS-TzBI** and **PBDTTS-TzBI**:ITIC films excited at 600 nm and a pure ITIC film excited at 700 nm.

To study the charge recombination mechanism, the variation of J_{sc} as a function of light intensity (P_{in}, from dark to 100 mW cm^{-2}) was analyzed. The dependence of J_{sc} on P_{in} is expressed as $J_{sc} \propto P_{in}^{\alpha}$, where α is obtained by fitting the data. When α is close to 1, bimolecular recombination at short-circuit becomes negligable.[66] The values of α are determined to be 0.94 and 0.98 for the devices based on **PBDTTSi-TzBI**:ITIC and **PBDTTS-TzBI**:ITIC, respectively. The higher α value of 0.98 suggests that charge carriers are swept out of the device more efficiently before bimolecularly recombining in the **PBDTTS-TzBI**:ITIC solar cells as compared to the **PBDTTSi-TzBI**:ITIC ones. These findings agree with the higher FF and performance of these devices (Table 2).[66, 68]

15

To gain additional insight into the charge recombination dynamics in the photoactive layer, the V_{oc} was measured as a function of P_{in} (Figure 5c). In principle, if the slope of V_{oc} against $\ln(P_{in})$ is close to kT/q, bimolecular recombination is the primary process, while if the slope is close to $2kT/q$, trap-assisted recombination is dominating (with k, T and q the Boltzmann constant, the temperature in Kelvin and the elementary charge, respectively).[69, 70] The calculated slopes are 1.49 and 1.19kT/q for the devices based on **PBDTTSi-TzBI**:ITIC and **PBDTTS-TzBI**:ITIC, respectively, suggesting that the alkylthiol side chains suppress trap-assisted recombination, resulting in a higher FF.

The minimum voltage loss (E_{loss}) in the conversion from photons to electrons for both the fullerene and non-fullerene devices was also determined using the equation $E_{loss} = E_{edge} - eV_{oc}$, where E_{edge} is a measure for the lowest photon energy of a strongly absorbed photon and is determined from the EQE spectrum (Figure S9, Table S7).[71-73] The E_{loss} of the fullerene-based solar cells is always above 1 eV, while that of the non-fullerene solar cells is below 1 eV.[38, 74] The device made from **PBDTTSi-TzBI** without processing additive nor thermal annealing afforded the lowest E_{loss} value of 0.69 eV.

Conclusions

In summary, two new high gap push-pull type copolymers – **PBDTTSi-TzBI** and **PBDTTS-TzBI**, based on an imide fused benzotriazole unit (TzBI) with linear and branched side chains and alkylsilyl (Si) or alkylthiol (S) substituted 4,8-di(thien-2-yl)benzo[1,2-*b*:4,5-*b'*]dithiophene (BDTT) – were designed and synthesized. The effect of the different side chains on the photovoltaic performance of the polymers was investigated in fullerene as well as non-fullerene polymer solar cells. The alkylsilyl substituted polymer showed a deeper HOMO level, which resulted in higher V_{oc} values around 1.0 V. On the other hand, the alkylthio substituted polymer showed a slightly broader and stronger absorption, a somewhat higher hole mobility and a higher J_{sc} and FF in polymer solar cells. The **PBDTTS-TzBI**:PC$_{71}$BM devices attained a PCE of 7.3%, while the **PBDTTSi-TzBI**:PC$_{71}$BM devices displayed rather modest efficiencies (up to 4.0%). The solar cell performances significantly improved upon using ITIC as the electron acceptor, which extended the absorption of the blends into the NIR and reduced the voltage losses. The inverted non-fullerene solar cells based on **PBDTTSi-TzBI**:ITIC showed a higher PCE of 6.9% as compared to the fullerene-based devices. The non-fullerene solar cells fabricated from

16

PBDTTS-TzBI:ITIC using 0.2% DPE as a processing additive and thermal annealing at 130 °C exhibited the highest PCE of 9.6%, which could be ascribed to a combination of strong and broad absorption and balanced charge carrier mobilities. This performance is among the highest efficiencies for non-fullerene polymer solar cells based on TzBI-containing polymer donors.[38, 39, 63, 64] The results achieved here indicate that, at least in the presented case, it is difficult to tune the photoactive blends based on alkylsilyl-substituted push monomers to such an extent that the inherently increased V_{oc} values lead to enhanced device efficiencies. In this respect, terpolymer or ternary blend strategies might be good alternative options.

Acknowledgments

Supplementary data

Experimental details (including polymer synthesis), TGA thermograms, solid-state UV-Vis-NIR absorption spectra, cyclic voltammograms, additional details on the solar cell fabrication and characterization (including optimization tables), space charge limited current fittings and determination of the voltage losses for strongly absorbed photons.

References

1. L. Lu, T. Zheng, Q. Wu, A. M. Schneider, D. Zhao and L. Yu, *Chem. Rev.*, 2015, **115**, 12666-12731.

2. G. Li, R. Zhu and Y. Yang, *Nat. Photonics*, 2012, **6**, 153.

3. W. Cao and J. Xue, *Energy Environ. Sci.*, 2014, **7**, 2123-2144.

4. S. Lizin, S. Van Passel, E. De Schepper, W. Maes, L. Lutsen, J. Manca and D. Vanderzande, *Energy Environ. Sci.*, 2013, **6**, 3136-3149.

5. S. Holliday, Y. Li and C. K. Luscombe, *Prog. Polym. Sci.*, 2017, **70**, 34-51.

6. J. Zhao, Y. Li, G. Yang, K. Jiang, H. Lin, H. Ade, W. Ma and H. Yan, *Nat. Energy*, 2016, **1**, 15027.

7. T. Kumari, S. M. Lee, S.-H. Kang, S. Chen and C. Yang, *Energy Environ. Sci.*, 2017, **10**, 258-265.

8. I. Cardinaletti, J. Kesters, S. Bertho, B. Conings, F. Piersimoni, J. D'Haen, L. Lutsen, M. Nesladek, B. V. Mele, G. V. Assche, K. Vandewal, A. Salleo, D. Vanderzande, W. Maes and J. V. Manca, *J. Photon. Energy*, 2014, **4**, 040997.

9. H. Zhang, S. Li, B. Xu, H. Yao, B. Yang and J. Hou, *J. Mater. Chem. A*, 2016, **4**, 18043-18049.

10. C. B. Nielsen, S. Holliday, H. Y. Chen, S. J. Cryer and I. McCulloch, *Acc. Chem. Res.*, 2015, **48**, 2803.

11. W. Zhao, D. Qian, S. Zhang, S. Li, O. Inganäs, F. Gao and J. Hou, *Adv. Mater.*, 2016, **28**, 4734.

12. J. Hou, O. Inganäs, R. H. Friend and F. Gao, *Nat. Mater.*, 2018, **17**, 119.

13. X. Li, X. Liu, W. Zhang, H.-Q. Wang and J. Fang, *Chem. Mater.*, 2017, **29**, 4176-4180.

14. H. Li, T. Earmme, G. Ren, A. Saeki, S. Yoshikawa, N. M. Murari, S. Subramaniyan, M. J. Crane, S. Seki and S. A. Jenekhe, *J. Am. Chem. Soc.*, 2014, **136**, 14589-14597.

15. F. Zhao, S. Dai, Y. Wu, Q. Zhang, J. Wang, L. Jiang, Q. Ling, Z. Wei, W. Ma, W. You, C. Wang and X. Zhan, *Adv. Mater.*, 2017, **29**, 1700144.

16. H. Yao, L. Ye, J. Hou, B. Jang, G. Han, Y. Cui, G. M. Su, C. Wang, B. Gao, R. Yu, H. Zhang, Y. Yi, H. Y. Woo, H. Ade and J. Hou, *Adv. Mater.*, 2017, **29**, 1700254.

17. S. Li, L. Ye, W. Zhao, S. Zhang, S. Mukherjee, H. Ade and J. Hou, *Adv. Mater.*, 2016, **28**, 9423-9429.

18. A. Wadsworth, M. Moser, A. Marks, M. S. Little, N. Gasparini, C. J. Brabec, D. Baran and I. McCulloch, *Chem. Soc. Rev.*, 2019, **48**, 1596-1625

19. Y. Lin, J. Wang, Z. G. Zhang, H. Bai, Y. Li, D. Zhu and X. Zhan, *Adv. Mater.*, 2015, **27**, 1170-1174.

20. W. Zhao, S. Li, H. Yao, S. Zhang, Y. Zhang, B. Yang and J. Hou, *J. Am. Chem. Soc.*, 2017, **139**, 7148-7151.

21. J. Yuan, Y. Zhang, L. Zhou, G. Zhang, H.-L. Yip, T.-K. Lau, X. Lu, C. Zhu, H. Peng, P. A. Johnson, M. Leclerc, Y. Cao, J. Ulanski, Y. Li and Y. Zou, *Joule*, 2019, **3**, 1140-1151.

22. B. Fan, D. Zhang, M. Li, W. Zhong, Z. Zeng, L. Ying, F. Huang and Y. Cao, *Sci. China Chem.*, 2019, **62**, 746-752.

23. L. Meng, Y. Zhang, X. Wan, C. Li, X. Zhang, Y. Wang, X. Ke, Z. Xiao, L. Ding, R. Xia, H.-L. Yip, Y. Cao and Y. Chen, *Science*, 2018, **361**, 1094-1098.

24. J. Chen and Y. Cao, *Acc. Chem. Res.*, 2009, **42**, 1709-1718.

25. E. Wang, W. Mammo and M. R. Andersson, *Adv. Mater.*, 2014, **26**, 1801-1826.

26. X. Wen, B. Xiao, A. Tang, J. Hu, C. Yang and E. Zhou, *Chin. J. Chem .* 2018, **36**, 392-398.

27. Y. Chen, Z. Du, W. Chen, Q. Liu, L. Sun, M. Sun and R. Yang, *Org. Electron.*, 2014, **15**, 405-413.

28. L. Feng, J. Yuan, Z. Zhang, H. Peng, Z.-G. Zhang, S. Xu, Y. Liu, Y. Li and Y. Zou, *ACS Appl. Mater. Interfaces*, 2017, **9**, 31985-31992.

29. A. Tang, F. Chen, B. Xiao, J. Yang, J. Li, X. Wang and E. Zhou, *Front. Chem.*, 2018, **6**, 147.

30. A. Tang, B. Xiao, Y. Wang, F. Gao, K. Tajima, H. Bin, Z.-G. Zhang, Y. Li, Z. Wei and E. Zhou, *Adv. Funct. Mater.*, 2018, **28**, 1704507.

31. Z. Liu, D. Liu, K. Zhang, T. Zhu, Y. Zhong, F. Li, Y. Li, M. Sun and R. Yang, *J. Mater. Chem. A*, 2017, **5**, 21650-21657.

32. H. Bin, L. Gao, Z.-G. Zhang, Y. Yang, Y. Zhang, C. Zhang, S. Chen, L. Xue, C. Yang, M. Xiao and Y. Li, *Nat. Commun.*, 2016, **7**, 13651.

33. L. Xue, Y. Yang, J. Xu, C. Zhang, H. Bin, Z.-G. Zhang, B. Qiu, X. Li, C. Sun, L. Gao, J. Yao, X. Chen, Y. Yang, M. Xiao and Y. Li, *Adv. Mater.*, 2017, **29**, 1703344.

34. S. C. Price, A. C. Stuart, L. Yang, H. Zhou and W. You, *J. Am. Chem. Soc.*, 2011, **133**, 4625-4631.

35. L. Lan, Z. Chen, Q. Hu, L. Ying, R. Zhu, F. Liu, T. P. Russell, F. Huang and Y. Cao, *Adv. Sci.*, 2016, **3**, 1600032.

36. C. B. Nielsen, R. S. Ashraf, N. D. Treat, B. C. Schroeder, J. E. Donaghey, A. J. P. White, N. Stingelin and I. McCulloch, *Adv. Mater.*, 2015, **27**, 948-953.

37. B. Fan, K. Zhang, X. F. Jiang, L. Ying, F. Huang and Y. Cao, *Adv. Mater.*, 2017, **29**, 1606396.

38. P. Zhu, B. Fan, X. Du, X. Tang, N. Li, F. Liu, L. Ying, Z. Li, W. Zhong, C. J. Brabec, F. Huang and Y. Cao, *ACS Appl. Mater. Interfaces*, 2018, **10**, 22495-22503.

39. B. Fan, X. Du, F. Liu, W. Zhong, L. Ying, R. Xie, X. Tang, K. An, J. Xin, N. Li, W. Ma, C. J. Brabec, F. Huang and Y. Cao, *Nat. Energy*, 2018, **3**, 1051-1058.

40. P. Verstappen, J. Kesters, L. D'Olieslaeger, J. Drijkoningen, I. Cardinaletti, T. Vangerven, B. J. Bruijnaers, R. E. M. Willems, J. D'Haen, J. V. Manca, L. Lutsen, D. J. M. Vanderzande and W. Maes, *Macromolecules*, 2015, **48**, 3873-3882.

41. P. Liu, S. Dong, F. Liu, X. Hu, L. Liu, Y. Jin, S. Liu, X. Gong, T. P. Russell, F. Huang and Y. Cao, *Adv. Funct. Mater.*, 2015, **25**, 6458-6469.

42. H. Wu, B. Zhao, W. Wang, Z. Guo, W. Wei, Z. An, C. Gao, H. Chen, B. Xiao, Y. Xie, H. Wu and Y. Cao, *J. Mater. Chem. A*, 2015, **3**, 18115-18126.

43. T. Liu, X. Pan, X. Meng, Y. Liu, D. Wei, W. Ma, L. Huo, X. Sun, T. H. Lee, M. Huang, H. Choi, J. Y. Kim, W. C. H. Choy and Y. Sun, *Adv. Mater.*, 2017, **29**, 1604251.

44. H. Yao, L. Ye, H. Zhang, S. Li, S. Zhang and J. Hou, *Chem. Rev.*, 2016, **116**, 7397-7457.

45. S. Zhang, L. Ye and J. Hou, *Adv. Energy Mater.*, 2016, **6**, 1502529.

46. S. Zhang, Y. Qin, J. Zhu and J. Hou, *Adv. Mater.*, 2018, **30**, 1800868.

47. Z. Genene, J. Wang, X. Meng, W. Ma, X. Xu, R. Yang, W. Mammo and E. Wang, *Adv. Electron. Mater.*, 2016, **2**, 1600084.

48. D. Lee, S. W. Stone and J. P. Ferraris, *Chem. Commun.*, 2011, **47**, 10987-10989.

49. D. Lee, E. Hubijar, G. J. D. Kalaw and J. P. Ferraris, *Chem. Mater.*, 2012, **24**, 2534-2540.

50. H. Bin, Z.-G. Zhang, L. Gao, S. Chen, L. Zhong, L. Xue, C. Yang and Y. Li, *J. Am.Chem. Soc.*, 2016, **138**, 4657-4664.

51. C. Cui, W.-Y. Wong and Y. Li, *Energy Environ. Sci.*, 2014, **7**, 2276-2284.

52. X. Xu, T. Yu, Z. Bi, W. Ma, Y. Li and Q. Peng, *Adv. Mater.*, 2018, **30**, 1703973.

53. B. Huang, L. Chen, X. Jin, D. Chen, Y. An, Q. Xie, Y. Tan, H. Lei and Y. Chen, *Adv. Funct. Mater.*, 2018, **28**, 1800606.

54. W. Liu, J. Zhang, Z. Zhou, D. Zhang, Y. Zhang, S. Xu and X. Zhu, *Adv. Mater.*, 2018, **30**, 1800403.

55. Z. Luo, H. Bin, T. Liu, Z.-G. Zhang, Y. Yang, C. Zhong, B. Qiu, G. Li, W. Gao, D. Xie, K. Wu, Y. Sun, F. Liu, Y. Li and C. Yang, *Adv. Mater.*, 2018, **30**, 1706124.

56. J.-S. Wu, S.-W. Cheng, Y.-J. Cheng and C.-S. Hsu, *Chem. Soc. Rev.*, 2015, **44**, 1113-1154.

57. H. Bin, Y. Yang, Z. Peng, L. Ye, J. Yao, L. Zhong, C. Sun, L. Gao, H. Huang, X. Li, B. Qiu, L. Xue, Z.-G. Zhang, H. Ade and Y. Li, *Adv. Energy Mater.*, 2018, **8**, 1702324.

58. B. A. Abdulahi, X. Xu, P. Murto, O. Inganäs, W. Mammo and E. Wang, *ACS Appl. Energy Mater.*, 2018, **1**, 2918-2926.

59. Q. Wang, S. Zhang, B. Xu, L. Ye, H. Yao, Y. Cui, H. Zhang, W. Yuan and J. Hou, *Chem. Asian J.*, 2016, **11**, 2650-2655.

60. Z. He, C. Zhong, S. Su, M. Xu, H. Wu and Y. Cao, *Nat. Photon.*, 2012, **6**, 591.

61. N. K. Elumalai, C. Vijila, R. Jose, A. Uddin and S. Ramakrishna, *Mater. Renew. Sustain. Energy* 2015, **4**, 11.

62. N. C. Das, S. Biswas and P. E. Sokol, *J. Renew. Sustain. Energy*, 2011, **3**, 033105.

63. B. Fan, K. Zhang, X.-F. Jiang, L. Ying, F. Huang and Y. Cao, *Adv. Mater.*, 2017, **29**, 1606396.

64. L. Lan, P. Cai, Y. Mai, Z. Hu, W. Wen, J. Zhang, Y. Li, H. Shi and J. Zhang, *Dyes and Pigments*, 2018, **158**, 219-224.

65. V. D. Mihailetchi, J. Wildeman and P. W. M. Blom, *Phys. Rev. Lett.*, 2005, **94**, 126602.

66. W. Gao, T. Liu, R. Ming, Z. Luo, K. Wu, L. Zhang, J. Xin, D. Xie, G. Zhang, W. Ma, H. Yan and C. Yang, *Adv. Funct. Mater.*, 2018, **28**, 1803128.

67. N. Bauer, Q. Zhang, J. Zhao, L. Ye, J.-H. Kim, I. Constantinou, L. Yan, F. So, H. Ade, H. Yan and W. You, *J. Mater. Chem. A*, 2017, **5**, 4886-4893.

68. A. K. K. Kyaw, D. H. Wang, V. Gupta, W. L. Leong, L. Ke, G. C. Bazan and A. J. Heeger, *ACS Nano*, 2013, **7**, 4569-4577.

69. O. G. Reid, H. Xin, S. A. Jenekhe and D. S. Ginger, *J. Appl. Phys.*, 2010, **108**, 084320.

70. Q. Fan, Q. Zhu, Z. Xu, W. Su, J. Chen, J. Wu, X. Guo, W. Ma, M. Zhang and Y. Li, *Nano Energy*, 2018, **48**, 413-420.

71. V. C. Nikolis, J. Benduhn, F. Holzmueller, F. Piersimoni, M. Lau, O. Zeika, D. Neher, C. Koerner, D. Spoltore and K. Vandewal, *Adv. Energy Mater.*, 2017, **7**, 1700855.

72. Y. Wang, D. Qian, Y. Cui, H. Zhang, J. Hou, K. Vandewal, T. Kirchartz and F. Gao, *Adv. Energy Mater.*, 2018, **8**, 1801352.

73. K. Vandewal, J. Benduhn and V. C. Nikolis, *Sustain. Energy Fuels*, 2018, **2**, 538-544.

74. A. Negash, Z. Genene, R. Thiruvallur Eachambadi, J. Kesters, N. Van den Brande, J. D'Haen, H. Penxten, B. A. Abdulahi, E. Wang, K. Vandewal, W. Maes, W. Mammo, J. Manca and S. Admassie, *J. Mater. Chem. C*, 2019, **7**, 3375-3384.